

A very massive neutron star: relativistic Shapiro delay measurements of PSR J0740+6620

H. T. Cromartie^{*1}, E. Fonseca², S. M. Ransom³, P. B. Demorest⁴, Z. Arzoumanian⁵, H. Blumer^{6,7}, P. R. Brook^{6,7}, M. E. DeCesar⁸, T. Dolch⁹, J. A. Ellis¹⁰, R. D. Ferdman¹¹, E. C. Ferrara¹², N. Garver-Daniels^{6,7}, P. A. Gentile^{6,7}, M. L. Jones^{6,7}, M. T. Lam^{6,7}, D. R. Lorimer^{6,7}, R. S. Lynch¹³, M. A. McLaughlin^{6,7}, C. Ng^{14,15}, D. J. Nice⁸, T. T. Pennucci¹⁶, R. Spiewak¹⁷, I. H. Stairs¹⁴, K. Stovall⁴, J. K. Swiggum¹⁸, & W. W. Zhu¹⁹

1. *Department of Astronomy, University of Virginia, 530 McCormick Rd., Charlottesville, VA 22903, USA*
2. *Department of Physics, McGill University, 3600 University St., Montreal, QC H3A 2T8, Canada*
3. *National Radio Astronomy Observatory, 520 Edgemont Rd., Charlottesville, VA 22903, USA*
4. *National Radio Astronomy Observatory, 1003 Lopezville Rd., Socorro, NM 87801, USA*
5. *X-ray Astrophysics Laboratory, Code 662, NASA Goddard Space Flight Center, Greenbelt, MD, 20771*
6. *Department of Physics and Astronomy, West Virginia University, P.O. Box 6315, Morgantown, WV 26506, USA*
7. *Center for Gravitational Waves and Cosmology, West Virginia University, Chestnut Ridge Research Building, Morgantown, WV 26505, USA*
8. *Department of Physics, Lafayette College, Easton, PA 18042, USA*
9. *Department of Physics, Hillsdale College, 33 E. College Street, Hillsdale, Michigan 49242, USA*
10. *Infinia ML, 202 Rigsbee Avenue, Durham NC, 27701*
11. *School of Chemistry, University of East Anglia, Norwich, NR4 7TJ, United Kingdom*
12. *NASA Goddard Space Flight Center, Greenbelt, MD 20771, USA*
13. *Green Bank Observatory, P.O. Box 2, Green Bank, WV 24944, USA*
14. *Department of Physics and Astronomy, University of British Columbia, 6224 Agricultural Road, Vancouver, BC V6T 1Z1, Canada*
15. *Dunlap Institute, University of Toronto, 50 St. George St., Toronto, ON M5S 3H4, Canada*
16. *Hungarian Academy of Sciences MTA-ELTE “Extragalactic Astrophysics Research Group”, Institute of Physics, Eötvös Loránd University, Pázmány P. s. 1/A, 1117 Budapest, Hungary*
17. *Centre for Astrophysics and Supercomputing, Swinburne University of Technology, P.O. Box 218, Hawthorn, Victoria 3122, Australia*
18. *Center for Gravitation, Cosmology and Astrophysics, Department of Physics, University of Wisconsin-Milwaukee, P.O. Box 413, Milwaukee, WI 53201, USA*
19. *CAS Key Laboratory of FAST, NAOC, Chinese Academy of Sciences, Beijing 100101, China*

Despite its importance to our understanding of physics at supranuclear densities, the equation of state (EoS) of matter deep within neutron stars remains poorly understood. Millisecond pulsars (MSPs) are among the most useful astrophysical objects in the Universe for such tests of fundamental physics, and continue to place some of the most stringent constraints on this high-density EoS. Pulsar timing — the process of accounting for every rotation of a pulsar over long time periods — can precisely measure a wide variety of physical phenomena (see, for example, [1]), including those that allow the measurement of the masses of the components of a pulsar binary system. One of these, called relativistic Shapiro delay [2], can yield precise masses for both an MSP and its companion; however, it is only easily observed in a small subset of highly inclined (nearly edge-on) binary pulsar systems. By combining data from the North American Nanohertz Observatory for Gravitational Waves (NANOGrav) 12.5-year data set with recent orbital-phase-specific observations using the Green Bank Telescope, we have measured the mass of the MSP J0740+6620 to be $2.17_{-0.10}^{+0.11}$ solar masses (68.3% credibility interval). It may therefore be the most massive neutron star yet observed, and would serve as a strong constraint on the neutron star interior EoS.

Relativistic Shapiro delay, which is observable when a pulsar passes behind its stellar companion during orbital conjunction, manifests as a small delay in pulse arrival times induced by the curvature of spacetime in the vicinity of the companion star. For a highly inclined MSP-white dwarf binary,

the full delay is of order $\sim 10 \mu\text{s}$. The relativistic effect is characterized by two parameters, “shape” and “range.” In general relativity, shape (s) is the sine of the angle of inclination of the binary orbit (i), while range (r) is proportional to the mass of the companion, m_c . When combined with the Keplerian mass function, measurements of r and s also constrain the pulsar mass (m_p ; [3] provides a detailed overview and an alternate parameterization).

Precise neutron star mass measurements are an effective way to constrain the equation of state (EoS) of the ultra-dense matter in neutron star interiors. Although radio pulsar timing cannot directly determine neutron star radii, the existence of pulsars with masses exceeding the maximum mass allowed by a given model can straightforwardly rule out that EoS.

In 2010, Demorest et al. reported the discovery of a 2-solar-mass MSP, J1614–2230¹ [5]. This Shapiro-delay-enabled measurement disproved the plausibility of some hyperon, boson, and free quark models in nuclear-density environments. In 2013, Antoniadis et al. used optical techniques in combination with pulsar timing to yield a mass measurement of $2.01 \pm 0.04 M_\odot$ for the pulsar J0348+0432 [6]. These two observational results (along with others; see [7]) encouraged a reconsideration of the canonical $1.4 M_\odot$ neutron star. Gravitational wave astrophysics has also begun to provide EoS constraints; for example, the Laser Interferometer Gravitational-Wave Observatory (LIGO) detection of a double neutron star merger constrains permissible equations of state, suggesting that the upper limit on neutron star mass is $2.17 M_\odot$ (90% credibility; [8]). Though the existence of extremely massive ($> 2.4 M_\odot$) neutron stars has been suggested through optical spectroscopic and photometric observations (e.g. [9]), radio timing can provide much more precise constraints on the existence of $\gtrsim 2 M_\odot$ neutron stars.

NANOGrav employs pulsar timing for an important general relativistic application: the detection of low-frequency gravitational waves primarily from supermassive black hole binaries. The collaboration’s observing program consists of high-cadence, multi-frequency radio observations of ~ 75 MSPs using the Green Bank and Arecibo telescopes² (GBT and AO; see [10] and the upcoming 12.5-year data release). Using the Green Bank Telescope, NANOGrav regularly observes J1614–2230 and another high-mass radio MSP, J0740+6620.

PSR J0740+6620 (period = 2.89 ms) was discovered in the Green Bank Northern Celestial Cap 350-MHz survey (GBNCC) in 2012 [11]. It is in a nearly circular (eccentricity = 5×10^{-6}), 4.77-day orbit.³ Recent optical and near-infrared observations by Beronya et al. (2019) revealed that its companion is likely the reddest white dwarf ever measured in orbit with an MSP ([13]).

Here we present timing observations of the pulsar with the Green Bank Telescope taken between 2014 and 2019. We observed the pulsar regularly throughout this period as part of the NANOGrav timing program ([10]). This section of our data set includes ~ 70 epochs (occurring approximately monthly and at random orbital phases) during which the pulsar was observed at both 1.4 GHz and 820 MHz for ~ 20 minutes each. We were awarded additional time for two concentrated campaigns over superior conjunction (i.e. when the pulsar is behind its companion star), as probing the minima and maxima of the Shapiro delay signal is the best way to improve sensitivity to it (see the absorbed or “detectable” signal in the second panel of Figure 1).

After the second concentrated campaign consisting of two five-hour observations at orbital phases 0.15 and 0.25 (GBT 18B–372), the timing analysis (see details in Methods) yielded a pulsar mass of $2.17^{+0.11}_{-0.10} M_\odot$ at 68.3% credibility. The Methods section describes our rationale for choosing these two orbital phases, as well as the progression of mass measurements and precisions as more

¹Though the originally reported mass was $1.97 \pm 0.04 M_\odot$, continued timing has led to a more precise mass measurement of $1.928 \pm 0.017 M_\odot$; Fonseca et al. 2016 [4].

²NANOGrav has recently begun using the Karl G. Jansky Very Large Array as the third observatory in its pulsar timing program.

³Lynch et al. presented a recent GBNCC timing solution in 2018 [12].

observations were added. Our final fits with and without Shapiro delay as a function of orbital phase are presented in Figure 1, and the top panel of Figure 2 shows timing residuals spanning the entire data set. Although our measured relative uncertainty is higher than, for example, the original relative error reported by Demorest et al. for J1614–2230 (5% vs. 2%), J0740+6620 is a remarkably high-mass MSP. This measurement will help constrain high-density nuclear physics, as there are very few examples of $\gtrsim 2 M_{\odot}$ neutron stars and because, at the moment, it appears likely to be the highest neutron star mass measured to date.

The discovery of increasingly massive neutron stars necessitates stiffer EoS, which generally allow for higher maximum masses. There exist several proposed neutron star interior EoS that remain viable given the second-highest neutron star mass measurement, (J0348+0432, $2.01 \pm 0.04 M_{\odot}$) but that are called into question — at least at the $1\text{-}\sigma$ credibility level — by our J0740+6620 measurement, though only two among these are discussed in this work. Douchin & Haensel (2001; [14]) crafted a “unified” (accounting for both crust and core) model for the neutron star interior EoS based on Skyrme-type nuclear interactions (referred to as the Skyrme-Lyon, or SLy, model). SLy predicts a maximum neutron star mass of $2.05 M_{\odot}$ that is in possible tension with our $2.17^{+0.11}_{-0.10} M_{\odot}$ measurement lower bound. A similar situation arises with “H4,” one of the stiffer hyperon-based EoS from Lackey, Nayyar, and Owen (2006) [15]. This model allows only for a $2.03\text{-}M_{\odot}$ neutron star, which is significantly less than the lower bound of our $1\text{-}\sigma$ credibility interval. Read et al. (2008) provide a useful summary of many proposed neutron star EoS [16].

Constraining the mass of J0740+6620 carries two additional astrophysical benefits. Recent evidence from Antoniadis et al. (2016) [17] suggests that the distribution of MSP masses may be bimodal, implying that many more neutron stars with masses greater than $\sim 1.6 M_{\odot}$ may exist than previously supposed (see also [18]). PSR J0740+6620 serves as another data point in the effort to study the overall MSP population, which, along with measurements of properties like ages and magnetic fields (and if possible, optical observations of companions) could result in valuable improvements in our understanding of MSP binary evolution. Additionally, if this MSP is measured to be at the high end of our mass credibility interval, it may provide evidence that the creation of a stable, high-mass neutron star is possible through the merger of two low-mass neutron stars (in a LIGO-like gravitational wave event).

Though it will require significant additional observing time to improve upon our J0740+6620 measurement, high-cadence monitoring of the pulsar is a promising strategy. Daily observations with the Canadian Hydrogen Intensity Mapping Experiment (CHIME; see [19]) telescope, in conjunction with the present data set, have the potential to determine the mass of J0740+6620 with 2–3% precision within a year. Additionally, the Neutron Star Interior Composition Explorer (NICER) is observing J0740+6620 at X-ray wavelengths⁴. Modeling the thermal pulse profile of this MSP at X-ray energies will aid in constraining the mass and radius of J0740+6620. Continued collaboration with multifrequency observing programs will guarantee the steady improvement of this pulsar mass measurement in the long term.

Methods

Green Bank Telescope Observations. Both NANOGrav and targeted observations were conducted using the Green bank Ultimate Pulsar Processing Instrument (GUPPI, [20]). Observations at 1500 MHz were acquired with 800 MHz of bandwidth split into 512 frequency channels (to be scrunched to 64 channels each before analysis), sampling every $0.64 \mu\text{s}$. At an observing frequency of 820 MHz, 200 MHz of bandwidth over 128 channels was acquired with an identical sampling

⁴https://heasarc.gsfc.nasa.gov/docs/nicer/science_team_investigations/

Table 1. J0740+6620 Best-Fit Parameters

Pulsar name.....	J0740+6620
MJD range (MJD)	56640 – 58462
Number of TOAs.....	7419
Measured Quantities	
Ecliptic longitude, l (degrees).....	103.75913607(2)
Ecliptic latitude, b (degrees)	44.10248468(2)
Epoch of position & period determination (MJD) ...	57551.0
Proper motion in ecliptic longitude (mas yr ⁻¹).....	-2.74(3)
Proper motion in ecliptic latitude (mas yr ⁻¹)	-32.44(4)
Parallax (mas)	0.6(3)
Spin frequency, ν (Hz).....	346.5319964932128(6)
Spin frequency derivative, $\dot{\nu}$ (s ⁻²).....	-1.46388(3) × 10 ⁻¹⁵
Dispersion measure, DM (pc cm ⁻³)*.....	14.961787
Profile frequency dependency parameter, FD1	-1.18(4) × 10 ⁻⁵
Binary model.....	ELL1
Projected semi-major axis of orbit, x (lt-s).....	3.9775560(2)
Binary orbital period, P_b (days)	4.7669446191(1)
Epoch of ascending node, TASC (MJD)	57552.08324415(2)
EPS1 (first Laplace-Lagrange parameter), $\epsilon \sin \omega$...	-5.70(5) × 10 ⁻⁶
EPS2 (second Laplace-Lagrange parameter), $\epsilon \cos \omega$.	-1.89(3) × 10 ⁻⁶
Sine of inclination angle i	0.9990(2)
Companion mass, m_c (M _⊙).....	0.258(8)
Derived Parameters	
Orbital eccentricity, e	5.07(4) × 10 ⁻⁶
Longitude of periastron, ω (degrees)	244.3(3)
Epoch of Periastron, T0 (MJD)	57550.551(4)
Binary mass function (M _⊙).....	0.0029733870(4)
Pulsar mass (68.3% credibility interval, M _⊙).....	2.17 ^{+0.11} _{-0.10}
Pulsar mass (95.4% credibility interval, M _⊙).....	2.17 ^{+0.23} _{-0.20}
Companion mass (68.3% credibility interval, M _⊙)...	0.26 ^{+0.008} _{-0.008}
Companion mass (95.4% credibility interval, M _⊙)...	0.26 ^{+0.02} _{-0.02}
Inclination angle (68.3% credibility interval, degrees)	87.35 ^{+0.21} _{-0.23}
Inclination angle (95.4% credibility interval, degrees)	87.35 ^{+0.41} _{-0.48}

*Because this DM is an unfitted reference value, no error is reported. Values of DMX for each of the ~70 epochs are available upon request.

rate. These dual-polarization observations at both frequencies were coherently dedispersed at the known DM of 15.0 pc cm^{-3} . Data were processed using NANOGrav pipelines for consistency with the existing four-year-long NANOGrav J0740+6620 data set (see [21] for a thorough description of NANOGrav observing procedures, and [22] for a description of NANOGrav’s main data processing pipeline, `nanopipe`).

The Timing Model. The process of extracting pulse times of arrival (TOAs) and their subsequent modeling closely mirrors the procedure described in Arzoumanian et al. (2018, [10]). Raw data were recorded in the form of folded pulse profiles using the known J0740+6620 ephemeris. Profiles were integrated over ~ 20 – 30 minute intervals (yielding one or two TOAs per scrunched frequency interval for a normal NANOGrav observation, and ~ 10 for a long conjunction scan). For each of these intervals, many TOAs were then extracted from the entire observing bandwidth using a standard template and the PSRCHIVE⁵ software package. The pulsar timing packages TEMPO⁶ and TEMPO2⁷ were used for all model fitting.

In addition to the dispersion measure modeling described later in this section, fitted parameters included celestial coordinates, proper motion, spin frequency and its first derivative, and binary orbital parameters (see Table 1, which lists values fit with TEMPO). The overall RMS timing residual value was $1.5 \mu\text{s}$. We employed the ELL1 binary model, which includes projected semi-major axis length, binary orbital period, companion mass, orbital inclination, epoch of periastron, and the first and second Laplace-Lagrange parameters (ϵ_1 and ϵ_2 ; the orbital eccentricity multiplied by the sine and cosine of periastron longitude, respectively; [25]). The solar system ephemeris model used in our fits was NASA Jet Propulsion Laboratory’s DE436⁸, and the time standard used was BIPM2017.

Standard noise parameters are of three varieties: EFAC, EQUAD, and ECORR. These three parameters are calculated for each backend and receiver combination with Enterprise⁹, NANOGrav’s noise modeling software. EFAC is a multiplicative factor for TOA uncertainties that accounts for systematic differences in TOAs from different receivers or backends. EQUAD is a similar (though added in quadrature) value that accounts for statistical errors in the calculation of TOAs as well as white noise. ECORR is a frequency-correlated factor to account for pulse phase jitter. These noise terms are included in the joint likelihood for all fitted parameters, which are calculated using a Markov chain Monte Carlo-based routine. In our fits, we include an EFAC of 1.035 for L-band (1500-MHz) TOAs and 1.012 for 820-MHz TOAs. EQUAD for L-band was $0.00766 \mu\text{s}$, and $0.20464 \mu\text{s}$ for 820 MHz. ECORR values for L-band and 820-MHz TOAs were $0.32072 \mu\text{s}$ and $0.01525 \mu\text{s}$, respectively. Once we had conducted this analysis once, we tested (per standard NANOGrav procedure) whether a red noise signature was significant in the data. For J0740+6620, noise analysis from Enterprise indicated that a low-amplitude (0.308), steep-spectrum (-5.55) red noise was favored for this data set when using a Bayes factor of 100 as a minimum value to assess red noise model significance. The inclusion of red noise actually improved our constraint on m_p , decreasing the error by nearly 25%. This is likely due to other noise parameters trying to absorb some of the excess red noise; if EFAC, ECORR, or EQUAD is artificially inflated, the mass constraint will be more poorly determined.

Dispersion Measure Modeling. The complexity of modeling DM variations arising from a

⁵Source code in [23]; see <http://psrchive.sourceforge.net>.

⁶<http://tempo.sourceforge.net/>

⁷Source code in [24]; see <https://www.atnf.csiro.au/research/pulsar/tempo2/>.

⁸<https://naif.jpl.nasa.gov/pub/naif/JUN0/kernels/spk/de436s.bsp.1b1>

⁹<https://enterprise.readthedocs.io/en/latest/>

dynamic interstellar medium has been discussed at length in previous works (see, for example, Lam et al. 2016 and Jones et al. 2017 [26, 27]). We have adopted the standard NANOGrav piecewise-constant model for DM trends wherein each epoch of data is fit with a constant “DMX” value; in other words, each of these parameters is a deviation from some nominal DM and is fixed over a single epoch. The observation that J0740+6620’s DM behavior is somewhat smooth over the duration of our data set (see Figure 2) led us to attempt alternatively modeling the entire data set by fitting for only the first and second derivatives of DM. In theory, this approach could be advantageous given the ability of DMX to absorb Shapiro delay signals (thanks to the similar duration of conjunction and a DMX epoch). While this strategy does reduce the formal parameter uncertainties from the fit, both an F-test and an Akaike information criterion test strongly favor the DMX model over the quadratic DM fit. This indicates the DM variation is not fully characterized by a quadratic model, and parameter values (including pulsar mass) derived from this model are likely to have systematic biases not reflected in their formal uncertainties.

Simulations. Analysis of the NANOGrav 12.5-year data set without supplemental data yielded $m_p = 2.00 \pm 0.20 M_\odot$. After the initial 6-hour supplemental observation, we measured the mass of J0740+6620 to be $2.18 \pm 0.15 M_\odot$. In order to simulate future observations¹⁰, we first generated an arbitrary array of TOAs that mirror the desired observing cadence, starting date, etc. The TOAs were then fit (with pulsar timing software such as TEMPO or PINT¹¹) using the known parameters for J0740+6620. Residuals from this fit were then subtracted from the original TOAs to create “perfect” TOAs, to which stochastic noise was then added.

Two notable types of simulations were conducted. The first was an estimation of the improvement in our measurement of m_p given random orbital sampling (the “NANOGrav-only observation” scenario); this solidified our conclusion that the concentrated campaigns were necessary. The second served to optimize our observing strategy during a targeted orbital phase campaign by trying various permutations of orbital phase, number of observing sessions, and observing session lengths. The results of this simulation informed our GBT Director’s Discretionary Time request for five hours over conjunction and five hours in one of the Shapiro “troughs” (we were awarded time in the first trough — around orbital phase 0.15 — in addition to conjunction).

References

- [1] Lorimer, D. R. & Kramer, M. Handbook of Pulsar Astronomy. *Cambridge University Press*. (2005).
- [2] Shapiro, I. I. Fourth Test of General Relativity. *Phys. Rev. Lett.* **13**, 789-791 (1964).
- [3] Freire, P. C. C. & Wex, N. The orthometric parametrization of the Shapiro delay and an improved test of general relativity with binary pulsars. *Mon. Not. R. Astron. Soc.* **409**, 199-212 (2010).
- [4] Fonseca, E. et al. The NANOGrav Nine-year Data Set: Mass and Geometric Measurements of Binary Millisecond Pulsars. *Astrophys. J.* **832**, 167-??? (2016).

¹⁰In this case, the simulations were used both to confirm the constraining power of the concentrated Director’s Discretionary Time campaigns and to describe what constraints we may achieve with data beyond that which is presented here.

¹¹<https://github.com/nanograv/PINT>

- [5] Demorest, P. B., Pennucci, T., Ransom, S. M., Roberts, M. S. E. & Hessels, J. W. T. A two-solar-mass neutron star measured using Shapiro delay. *Nature*. **467**, 1081-1083 (2010).
- [6] Antoniadis, J. et al. A Massive Pulsar in a Compact Relativistic Binary. *Science*. **340**, 448-??? (2013).
- [7] Friere, P. C. C. et al. On the nature and evolution of the unique binary pulsar J1903+0327. *Mon. Not. R. Astron. Soc.* **412**, 2763-2780 (2011).
- [8] Margalit, B. & Metzger, B. D. Constraining the Maximum Mass of Neutron Stars From Multi-Messenger Observations of GW170817. *Astrophys. J. L.* **850**, L19-??? (2017).
- [9] Linares, M., Shahbaz, T., & Casares, J. Peering into the dark side: magnesium lines establish a massive neutron star in PSR J2215+5135. *Astrophys. J.* **859**, 54-??? (2018).
- [10] Arzoumanian, Z. et al. The NANOGrav 11-year Data Set: Pulsar-timing Constraints On The Stochastic Gravitational-wave Background. *Astrophys. J.* **859**, 47-??? (2018).
- [11] Stovall, K. et al. The Green Bank Northern Celestial Cap Pulsar Survey. I. Survey Description, Data Analysis, and Initial Results. *Astrophys. J.* **791**, 67-??? (2014).
- [12] Lynch, R. S. et al. The Green Bank North Celestial Cap Pulsar Survey. III. 45 New Pulsar Timing Solutions. *Astrophys. J.* **859**, 93-??? (2018).
- [13] Beronya, D. M. et al. The ultracool helium-atmosphere white dwarf companion of PSR J0740+6620?. *Submitted to MNRAS*, arXiv:1902.11150 (2019).
- [14] Douchin, F. & Haensel, P. A unified equation of state of dense matter and neutron star structure. *Astronomy & Astrophysics*. **380**, 151-167 (2001).
- [15] Lackey, B. D., Nayyar, M. & Owen, B. J. Observational constraints on hyperons in neutron stars. *Phys. Rev. D.* **73**, 024021(?) (2006).
- [16] Read, J. S. , Lackey, B. D. , Owen, B. J. , & Friedman, J. L. Constraints on a phenomenologically parametrized neutron-star equation of state. *Phys. Rev. D.* **79**, 124032(?) (2009).
- [17] Antoniadis, J. et al. The millisecond pulsar mass distribution: Evidence for bimodality and constraints on the maximum neutron star mass. record: arXiv:1605.01665 (2016).
- [18] Özel, F. & Freire, P. Masses, Radii, and the Equation of State of Neutron Stars. *Annual Review of Astronomy and Astrophysics*. **54**, 401-440 (2016).
- [19] Ng, C. Pulsar science with the CHIME telescope. *Pulsar Astrophysics the Next Fifty Years (IAU Symposium proceedings)*. **337**, 179-182 (2018).
- [20] DuPlain, R. et al. Launching GUPPI: the Green Bank Ultimate Pulsar Processing Instrument. *Advanced Software and Control for Astronomy II*. Edited by Bridger, A. & Radziwill, N. M. Proceedings of the SPIE, Volume 7019, article id. 70191D, 10 pp. (2008).
- [21] Arzoumanian, Z. et al. The NANOGrav Nine-Year Data Set: Observations, Arrival Time Measurements, and Analysis of 37 Millisecond Pulsars. *Astrophys. J.* **813**, 65-??? (2015).
- [22] Demorest, P. B. nanopipe: Calibration and data reduction pipeline for pulsar timing. *Astrophysics Source Code Library*, record: ascl:1803.004 (2018).

- [23] van Straten, W. et al. PSRCHIVE: Development Library for the Analysis of Pulsar Astronomical Data. *Astrophysics Source Code Library*, record: ascl:1105.014 (2011).
- [24] Hobbs, G. & Edwards, R. Tempo2: Pulsar Timing Package. *Astrophysics Source Code Library*, record: ascl:1210.015 (2012).
- [25] Lange, Ch. et al. Precision timing measurements of PSR J1012+5307. *Mon. Not. R. Astron. Soc.* **326**, 274-282 (2001).
- [26] Lam, M. T. et al. Systematic and Stochastic Variations in Pulsar Dispersion Measures. *Astrophys. J.* **821**, 66-??? (2015).
- [27] Jones, M. L. et al. The NANOGrav Nine-Year Data Set: Measurement and Interpretation of Variations in Dispersion Measures. *Astrophys. J.* **841**, 125-??? (2017).

Acknowledgements

The NANOGrav Project receives support from NSF Physics Frontiers Center award number 1430284. Pulsar research at UBC is supported by an NSERC Discovery Grant and by the Canadian Institute for Advanced Research (CIFAR). The National Radio Astronomy Observatory and the Green Bank Observatory are facilities of the National Science Foundation operated under cooperative agreement by Associated Universities, Inc. S.M.R is a CIFAR Senior Fellow. W.W.Z. is supported by the CAS Pioneer Hundred Talents Program, the Strategic Priority Research Program of the Chinese Academy of Sciences, grant No. XDB23000000, and the National Natural Science Foundation of China grant No. 11690024, 11743002, 11873067. Supplementary Green Bank conjunction-phase observing project codes were 18B-289 and 18B-372 (DDT).

Author Contributions

The creation of the NANOGrav 12.5-year data set was made possible through extensive observations and pulsar timing activities conducted by the authorship list in its entirety. H.T.C. was responsible for the NANOGrav-adjacent concentrated observing campaigns and the majority of this manuscript's contents. H.T.C., E.F., S.M.R., and P.B.D. were responsible for the extended J0740+6620 data analysis (the merging of NANOGrav and conjunction-phase observations) and modeling effort. E.F. was responsible for much of the initial work on J0740+6620 that informed the supplementary observing proposals, and for the development of the gridding code that yielded both the mass and inclination credibility intervals and Figure 3.

Competing Interests

The authors of this letter declare no competing interests.

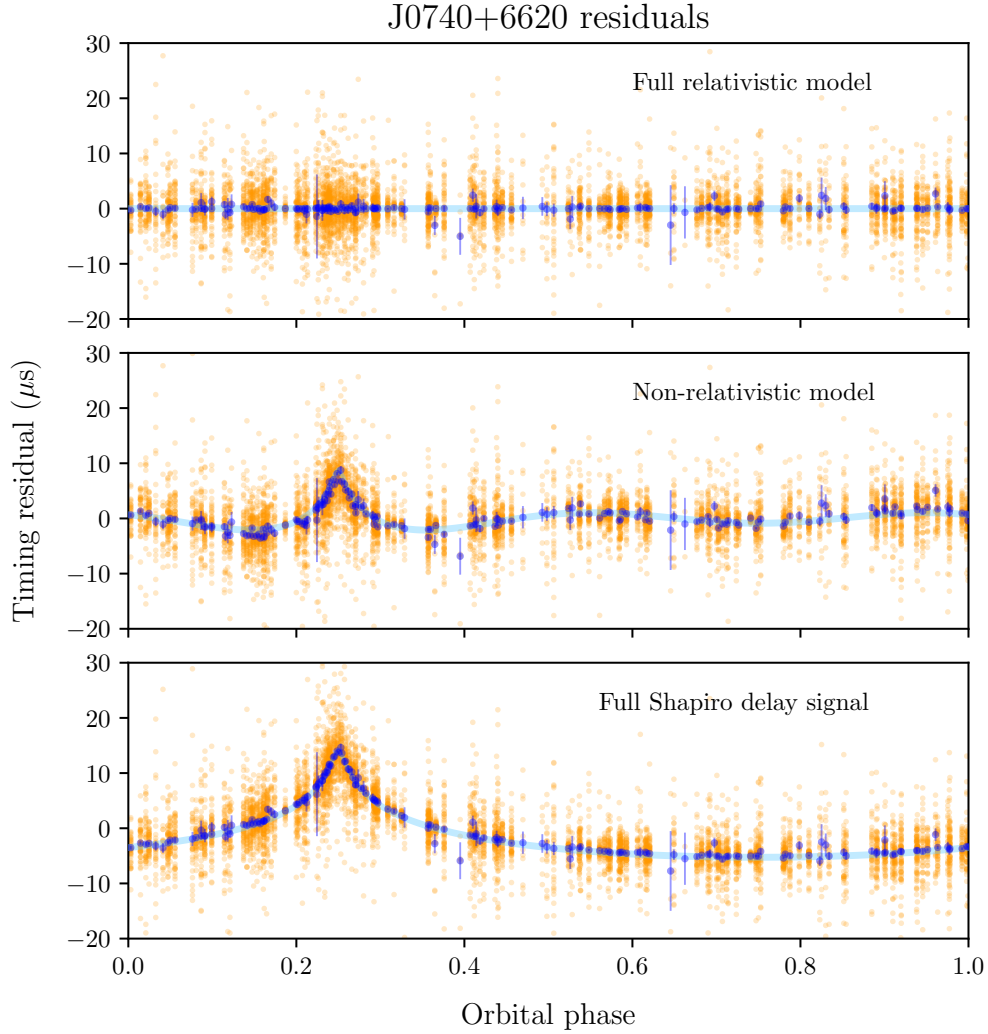


Figure 1 Timing residuals from all observations of J0740+6620 as a function of orbital phase, with superior conjunction at orbital phase = 0.25. Orange points are multi-frequency timing residuals, while blue points are averages of each group (i.e. timing epoch) of these points with error bars. The top panel shows a full fit including Shapiro delay parameters. The middle panel is the best fit without Shapiro parameters. The bottom panel is the “full” Shapiro signal using the best-fit Keplerian orbital (i.e. non-relativistic) parameters from the top panel. The lighter blue line in the middle and bottom panels represents the theoretical measurable and full Shapiro delay, respectively (and marks a $0\text{-}\mu\text{s}$ residual in the top panel). The width of the line in each panel is equal to the root mean squared error of the averaged points. A single averaged epoch (one dark blue point) was removed from these plots, as its error bar was $\sim 8\text{ }\mu\text{s}$ due to a faint detection from which only one TOA could be extracted.

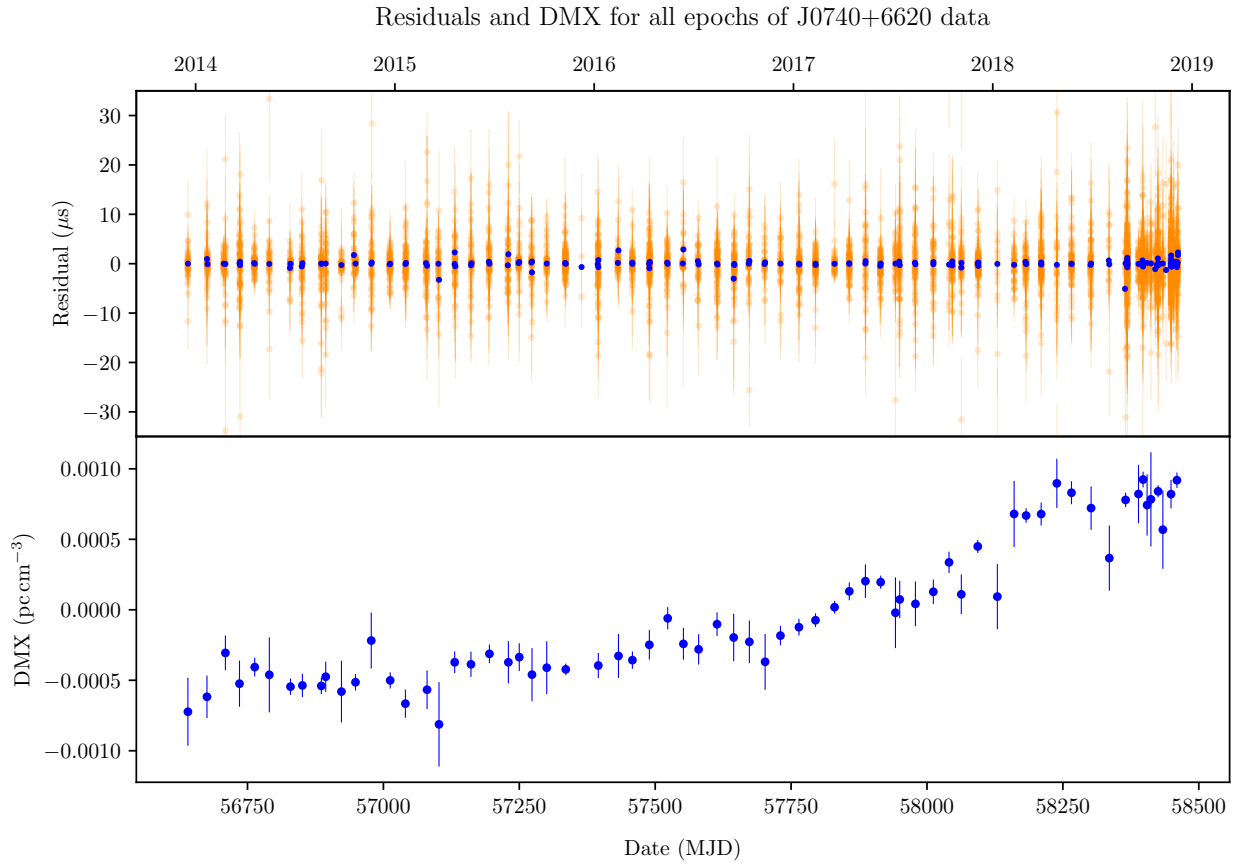


Figure 2 *Top panel*: residuals from all epochs of J0740+6620 data, including both NANOGrav and superior conjunction-specific observations at all frequencies, are shown in orange. The superimposed blue points represent an average over each epoch (RMS = $1.4 \mu\text{s}$; note that some days have two separately calculated averages from dual-frequency data). *Bottom panel*: Blue points indicate DMX values calculated for each epoch of data. The DMX trend is somewhat simple (i.e., roughly quadratic); however, linear modeling is strongly disfavored. For the reasons discussed in Figure 1, the same high-uncertainty epoch has been removed from these data.

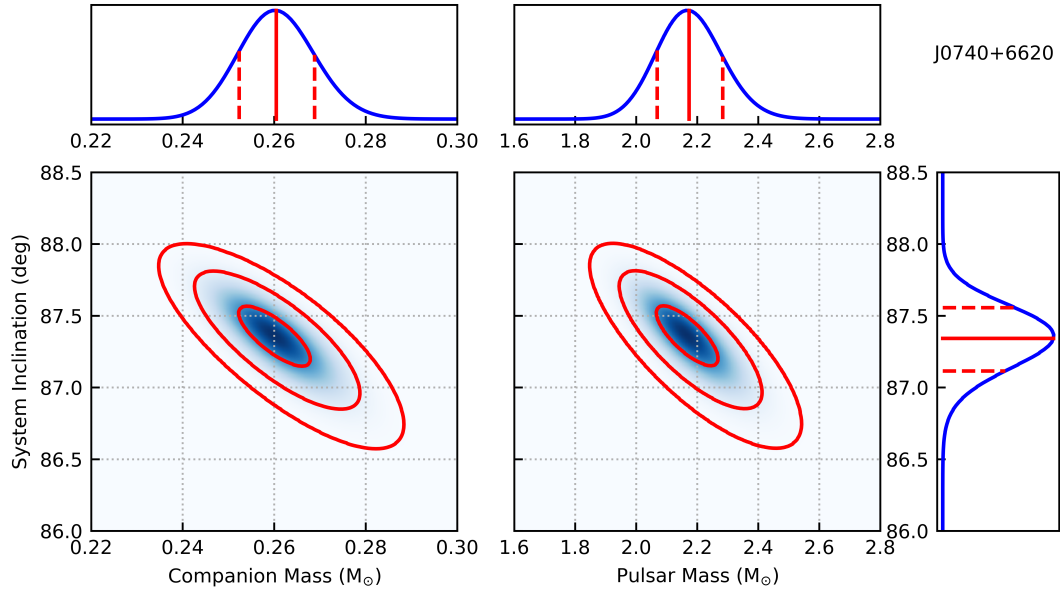


Figure 3 Map of fitted χ^2 distributions and corresponding probability density functions for m_p , m_c , and i . The left-hand heat map was generated by computing χ^2 values for different combinations of m_c and i ; the right-hand heat map was calculated by translating the $m_c - i$ probability density function to the $m_p - i$ phase space using the binary mass function. Darker blue regions correspond to lower χ^2 values. The three red circles correspond to 1, 2, and 3- σ significance cutoffs. Each of the three probability density functions (blue lines plotted on the tops and side of the heat maps) are projections of the χ^2 distributions. The solid red lines mark median values of each of the three parameters, while red dashed lines denote the upper and lower bounds of the 68.3% ($1-\sigma$) credibility interval.